Low-loss Ca$_{5-x}$Sr$_x$A$_2$TiO$_{12}$ [A=Nb,Ta] ceramics: Microwave dielectric properties and vibrational spectroscopic analysis

Pazhoor Varghese Bijumon and Mailadil Thomas Sebastian[a]
Ceramic Technology Division, Regional Research Laboratory, Trivandrum 695 019, India

Anderson Dias
*Departamento de Engenharia Metalúrgica e de Materiais, Universidade Federal de Minas Gerais (UFMG),
Rua Espírito Santo 35, Sala 206, Belo Horizonte Minas Gerais (MG) 30160-030, Brazil*

Roberto Luiz Moreira
*Departamento de Física, Instituto de Ciências Exatas (ICEx), Universidade Federal de Minas Gerais
(UFMG), C.P. 702, Belo Horizonte Minas Gerias (MG) 30123-970, Brazil*

Pezholil Mohanan
Department of Electronics, Cochin University of Science and Technology, Kochi-682 022, India

Complex perovskite-type Ca$_{5-x}$Sr$_x$A$_2$TiO$_{12}$ [A=Nb,Ta] ($0 \leq x \leq 5$) ceramics were prepared by conventional solid-state ceramic route. The crystal structure, microwave dielectric properties, and vibrational spectroscopic characteristics of these materials are reported. The structure and microstructure were investigated by x-ray diffraction and scanning electron microscopy techniques. The microwave dielectric properties were measured in the 3–5-GHz frequency range by the resonance method. Structural evolutions from orthorhombic to an averaged pseudocubic phase, with associated changes in dielectric properties, were observed as a function of composition. The structure-property relationships in these ceramics were established using Raman and Fourier transform infrared spectroscopic techniques. Raman analysis showed characteristic bands of ordered perovskite materials, with variation in both intensity and frequency as a function of composition. © 2005 American Institute of Physics. [DOI: 10.1063/1.1897065]

I. INTRODUCTION

The progress in wireless communication technology necessitated the development of microwave dielectric resonator (DR)[1,2] materials with high dielectric constant (ε_r), high unloaded quality factor (Q_u), and low-temperature coefficient of resonant frequency (τ_f). These rigorous dielectric property requirements preclude the use of all the available materials in microwave devices such as oscillators, filters, and dielectric resonator antennas. The versatility and adaptability of DRs have made them indispensable components in modern telecommunication systems. High-dielectric constant materials are also very important in microelectronic technologies such as dynamic random access memory (DRAM)[3] devices, substrates for microwave integrated circuits (MIC), and as gate dielectrics. Many different dielectric materials have been reported by several research groups. Because of the difficulty in controlling all the dielectric properties at microwave frequencies, intense work is going on in search of new materials with high ε_r, low dielectric loss (high Q_u), and low τ_f.

Complex perovskite oxide (ABO_3) materials[4–7] form a major class of dielectric resonator family, and have been extensively investigated because of their excellent microwave dielectric properties. Most of them have high quality factor and posses ε_r in the range 20–35. Materials having still high-dielectric constants are preferable because they can further

aid size reduction of the microwave circuit. Presently active work is being carried out in search of new materials[8,9] with improved properties, as well as tailoring the properties of existing materials by doping,[10,11] glass addition,[12,13] and solid solution formations.[14–17] Calcium- and strontium-based complex perovskites[18,19] are of special interest because they feature moderate dielectric constant and τ_f. Temperature-stable derivatives of these ceramics can be easily obtained by possible substitution in the perovskite A or B site.

In 1999, Cava *et al.*[20] reported the dielectric properties of Ca$_5$Nb$_2$TiO$_{12}$ and Ca$_5$Ta$_2$TiO$_{12}$ ceramics at 1 MHz. They proposed a pseudobinary phase diagram in the ABO_3 structure, where a mixing of three cations on the perovskite B site occurs and are represented as [Ca(Ca$_{1/4}$Nb$_{1/2}$Ti$_{1/4}$)O$_3$ and Ca(Ca$_{1/4}$Ta$_{1/2}$Ti$_{1/4}$)O$_3$]. Their results suggested that an order-disorder transition among the B-site ions plays a major role in the determination of temperature dependence of dielectric constant for both the compounds. Cava *et al.* found that different types of ordering between (111) planes, namely, 1:1, 1:2, and 1:3, as well as distortions by tilting of octahedra are involved in the formation of a microstructural state at room temperature.[21] While Ca$_5$Nb$_2$TiO$_{12}$ presents a 1:3 ordering, the analogous tantalum compound Ca$_5$Ta$_2$TiO$_{12}$ presents a 1:2 type of ordering. Recently, Bijumon *et al.*[22,23] studied the synthesizing conditions, structure, microstructure, and microwave dielectric properties of the Ca$_5$A$_2$TiO$_{12}$ (A=Nb,Ta) system. Ca$_5$Nb$_2$TiO$_{12}$ has ε_r=48, $Q_u \times f > 26\,000$ GHz (at 4 GHz) and τ_f=+40 ppm/°C, whereas Ca$_5$Ta$_2$TiO$_{12}$ has ε_r=38, $Q_u \times f > 33\,000$ GHz (at 4.5 GHz)

[a] Author to whom correspondence should be addressed; electronic mail: mailadils@yahoo.com

and $\tau_f = +10$ ppm/°C. The material has an orthorhombic structure and belongs to the *Pnma* space group[22] similar to the $CaTiO_3$ ceramics. Later, Benderski *et al.*[24] made a detailed investigation on the microstructural evolution and phase equilibrium of $Ca_5A_2TiO_{12}$ (A=Nb,Ta) ceramics and established a phase diagram with five single-phase fields related to each other by different cations. Efforts have been made to tailor the microwave dielectric properties,[25] especially to attain the temperature compensation of resonant frequency by solid solution formations in the above system, and to reduce its sintering temperature by glass fluxing.[26] This material has also been used to enhance the bandwidth of DR-loaded microstrip patch antennas,[27] and also find application in the fabrication of wideband dielectric resonator antennas.[28] Calcium-strontium solid solution formation[29–31] in the perovskite A site of the dielectric resonator material has attracted much attention because of their interesting structural and dielectric properties. In the present work we report the effect of Sr^{2+} substitution for Ca^{2+} in the perovskite A site of $Ca_{5-x}Sr_xA_2TiO_{12}$ (A=Nb,Ta) ceramics.

The extreme chemical and structural complexity of the system $Ca_5A_2TiO_{12}$ (A=Nb,Ta) indicate that additional studies must be carried out for an improved understanding of structure-property relationship. Also, the introduction of other isovalent metal ion in the system, such as strontium, could modify the structural and dielectric properties of these materials. In this respect, Raman and Fourier transform infrared spectroscopies were employed to investigate the vibrational properties that originated from the gradual substitution of Sr on the perovskite A site in place of Ca, as well as its effects on the metal-oxygen stretching/bending vibrations in $Ca_{5-x}Sr_xA_2TiO_{12}$ (A=Nb,Ta) ceramic systems.

II. EXPERIMENT

$Ca_{5-x}Sr_xNb_2TiO_{12}$ and $Ca_{5-x}Sr_xTa_2TiO_{12}$ ceramics were prepared by conventional solid-state route. High-purity (>99.9%) $CaCO_3$, $SrCO_3$, TiO_2 (Aldrich Chemical Company Inc., Milwaukee, WI, USA), and Ta_2O_5/Nb_2O_5 (Nuclear Fuel Complex, Hyderabad, India) were used as the starting materials. Stoichiometric amount of the oxides were weighed and ball milled, using zirconia balls in plastic containers and using distilled water as the wetting media, for 24 h. The slurry was dried in a glass bowl, in an oven kept at 90 °C, and the resultant reaction mixture was calcined in the temperature range 1240–1350 °C for 4 h in platinum crucibles. The powder was ground well and mixed with 4-wt % solution of poly(vinyl alcohol), PVA, as the binder. After drying and grounding into fine powder, the materials were then uniaxially pressed into cylindrical disks with 14-mm diameter and about 7-mm height under a pressure of 100 MPa. The ceramic pucks were placed over a platinum plate and sintered in the temperature range 1530–1625 °C for 4 h, with an intermediate firing at 800 °C to expel the organic binder. The sintered samples were well polished, and their bulk densities were calculated by the Archimedes method. Structural phases were identified by powder x-ray diffraction (XRD) technique (Philips X-ray diffractometer, Netherlands) using $CuK\alpha$ radiation. Scanning electron mi-

crographs (SEM S-2400, Hitachi, Japan) were recorded from the surface of sintered thermally etched samples to analyze the microstructure of the ceramics.

The microwave dielectric properties such as dielectric constant, unloaded quality factor, and the temperature coefficient of the resonant frequency were measured by using a HP8510C Vector Network Analyzer attached with a sweep oscillator and reflection transmission test unit. Q_u was measured using resonance method[32] by keeping the sample on a quartz spacer kept inside a copper cavity. Electromagnetic energy is fed into the cavity and coupled to the DR through two loop antennas. The $TE_{01\delta}$ mode, which is least perturbed by the cavity excitations, were used for the Q_u measurements. For the ceramics studied in the present work, resonance occurred between 3 to 5 GHz. The dielectric constant was measured by the Hakki–Coleman[33] post resonator method, later modified by Courtney.[34] The dielectric constant hence obtained by the Hakki–Colemann method was verified using the cavity method.[32] In the end-shorted position the sample was heated from room temperature to 80 °C, and the resonant frequency was noted at every 5 °C interval. The temperature variation of resonant frequency of the cylindrical DR can be calculated as

$$\tau_f = \frac{1}{f_{20}} \left\{ \frac{f_{80} - f_{20}}{60} \right\} \times 10^6 \text{ ppm/°C},$$

where f is the resonant frequency and the suffixes denote the temperature in °C.

Micro-Raman scattering spectra were recorded using a Horiba/Jobin–Yvon LABRAM-HR spectrometer, equipped with a 1800-grooves/mm diffraction grating, a liquid-N_2-cooled charge coupled device (CCD) detector, and a confocal microscope (100X objective). The experimental resolution was better than 1 cm^{-1}. After fitting, the ultimate resolution was 0.2 cm^{-1}. The measurements were carried out in back-scattering geometry at room temperature, using the 632.8-nm line of a helium-neon ion laser (power 12.5 mW) as excitation source. A holographic notch filter was used for stray light rejection (Rayleigh scattered light). The sample surfaces of the sintered materials were previously polished to an optical grade in order to improve the ratio of inelastic to elastic scattered light.

Infrared reflectance spectra were recorded in a Fourier transform spectrometer (Bomem DA8-02) equipped with a fixed-angle specular reflectance accessory (external incidence angle of 11.5°). The far-infrared range (50–500 cm^{-1}) was studied by using a mercury-arc lamp, a 6-μm coated Mylar® hypersplitter and LHe-cooled Si bolometer. In the mid-infrared region (500–4000 cm^{-1}) we used a globar source (SiC), a Ge-coated KBr beamsplitter, and a LN$_2$-cooled HgCdTe detector. One of the ceramic faces received a thin gold coating, and was used as a "rough" mirror for the reference spectra. This procedure allowed us to improve the reflectivity spectra, because the mirror surface mimics the sample one, which compensates the effects of diffuse reflection at the sample surface. The measurements were performed under low vacuum (10^{-3} bar) with a typical resolution of 2 cm^{-1}.
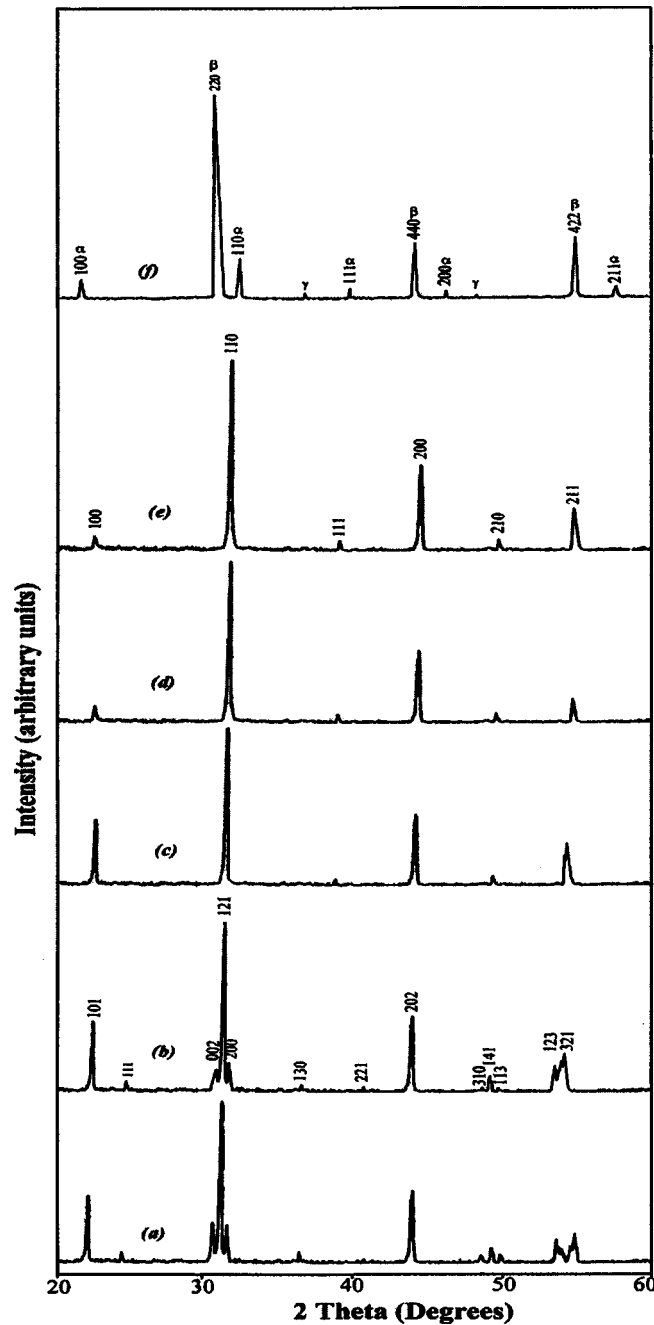
FIG. 1. X-ray diffraction pattern of (a) $Ca_5Nb_2TiO_{12}$, (b) $Ca_4SrNb_2TiO_{12}$, (c) $Ca_3Sr_2Nb_2TiO_{12}$, (d) $Ca_2Sr_3Nb_2TiO_{12}$, (e) $CaSr_4Nb_2TiO_{12}$, and (f) $Sr_4Nb_2O_9$–$SrTiO_3$ ceramics ($\alpha \rightarrow SrTiO_3$, $\beta \rightarrow Sr_4Nb_2O_9$, and $\gamma \rightarrow$ unidentified peaks).

FIG. 2. X-ray diffraction pattern of (a) $Ca_5Ta_2TiO_{12}$, (b) $Ca_4SrTa_2TiO_{12}$, (c) $Ca_3Sr_2Ta_2TiO_{12}$, (d) $Ca_2Sr_3Ta_2TiO_{12}$, (e) $CaSr_4Ta_2TiO_{12}$, and (f) $Sr_4Ta_2O_9$–$SrTiO_3$ ceramics ($\alpha \rightarrow SrTiO_3$, $\beta \rightarrow Sr_4Ta_2O_9$, and $\gamma \rightarrow$ unidentified peaks).

III. RESULTS AND DISCUSSION

A. Structural characterization

The XRD pattern of $Ca_{5-x}Sr_xNb_2TiO_{12}$ and $Ca_{5-x}Sr_xTa_2TiO_{12}$ ceramics are shown in Figs. 1 and 2, respectively. The patterns are similar for both Nb- and Ta-based ceramics. It is known that[35] in a perovskite structure, a bigger cation will occupy the A site of the perovskite structure, and hence in the present case, the compositions can be possibly represented as $Ca(Ca_{1/4}A_{2/4}Ti_{1/4})O_3$, $Ca_{3/4}Sr_{1/4}(Ca_{1/4}A_{2/4}Ti_{1/4})O_3$, $Ca_{2/4}Sr_{2/4}(Ca_{1/4}A_{2/4}Ti_{1/4})O_3$, $Ca_{1/4}Sr_{3/4}(Ca_{1/4}A_{2/4}Ti_{1/4})O_3$, and $Sr(Ca_{1/4}A_{2/4}Ti_{1/4})O_3$ for x

$=0$, 1, 2, 3, and 4, respectively, owing to the onset of the higher ionic radius[36] of Sr^{2+} compared with that of Ca^{2+}. The XRD profile of all compositions in the $Ca_{5-x}Sr_xA_2TiO_{12}$ ($A=Nb,Ta$) system were indexed based on the complex perovskite structure. However, it should be noted that XRD analysis alone is not enough to confirm A- or B-site substitution in the perovskite structure.

$Ca_5A_2Ti_1O_{12}$ and $Ca_4SrA_2TiO_{12}$ ($A=Nb,Ta$) have orthorhombic structures, with four formula units in the primitive cell and a regular alternation of B-site ions along the a, b, and c axes. Hence, the XRD patterns in Figs. 1 and 2 for the compositions with $x=0$ and 1 have been indexed based on the orthorhombic $Pnma$ symmetry.[22] The compositions with $x=2$ to 4, Figs. 1(c)–1(e) and 2(c)–2(e), presented an averaged cubic double-perovskite[37] $AA'(BB'B'')O_3$-type structure, with an occupancy of two cations in the A site (Ca, Sr

TABLE I. Synthesizing conditions, lattice parameters, cell volume, density, and tolerance factor of $Ca_{5-x}Sr_xNb_2TiO_{12}$ ($0 \leqslant x \leqslant 4$) and $Sr_4Nb_2O_9 - SrTiO_3$ ceramics.

| | Calcination temperature (°C) | Sintering temperature (°C) | Structure of the unit cell | Lattice parameters (Å) [Standard deviation SD=±0.0002 Å] | | | Cell volume (Å³) | Theoretical density (g/cm³) | % Density | Tolerance factor (t) |
x				a	b	c				
0	1350	1550	Orthorhombic	5.510 4	7.907 9	5.688 0	247.858 5	4.19	96.42	0.918 9
1	1300	1550	Orthorhombic	5.533 5	7.906 9	5.696 2	249.224 8	4.29	96.41	0.927 3
2	1275	1540	Pseudocubic	3.974 1	⋯	⋯	251.051 2	4.77	96.70	0.935 7
3	1275	1530	Pseudocubic	4.024 0	⋯	⋯	260.641 2	4.91	96.21	0.944 1
4	1260	1530	Pseudocubic	4.043 6	⋯	⋯	264.115 7	5.13	98.66	0.952 5
5	1240	1550	Mixture ($Sr_4Nb_2O_9-SrTiO_3$)	a	a	a	a	a	a	a

[a]Could not be calculated because of the mixed-phase nature.

for $x=2$ and 3; and Sr for $x=4$) and three cations in the B site (Ca, Nb/Ta, Ti). In order to obtain their structural parameters, their main reflections were indexed, comparing with the XRD profile of $Ba(Zn_{1/3}Nb_{2/3})O_3$ (ICDD File 17–182). For $x=2$ to 4, the XRD profiles consist of strong peaks characteristics of the primitive $Pm3m$ cubic perovskite, together with extra lines arising from superlattice reflections. However, XRD patterns are not accurate enough to assure that a structural phase transition from $Pnma$ to $Pm3m$ takes place when x varies from 1 to 2 in both $Ca_{5-x}Sr_xNb_2TiO_{12}$ and $Ca_{5-x}Sr_xTa_2TiO_{12}$ ceramics. Indeed, as we can observe in Figs. 1(c) and 2(c) (both for $x=2$), the (123) and (321) orthorhombic peaks are still present in the diffractograms, but they became too close. A similar effect can be observed for the orthorhombic (200) and (002) peaks that merge with the (121) peak into the experimental resolution. For higher x values ($x=3$ and 4), x-ray diffractometry is no longer able to distinguish between a true cubic structure and a pseudocubic one, where the orthorhombic ferroelastic distortion became too small. This difficulty could be overcome by the study of the local symmetries by spectroscopic techniques, as it will be shown in the corresponding sections below. With the in-troduction of larger Sr^{2+} ions, the anisotropic cell expansion decreases the differences between the lattice parameters and the structure evolves from a clear orthorhombic to a pseudocubic structure, but the space group remains $Pnma$. The effect of the radius of the substituted cation is still more important for $x=5$. Indeed, Sr^{2+} is too large to enter into the B site of the perovskite structure, so that this structure is not formed. Instead, a mixture of $Sr_4A_2O_9$ ($A=Nb, Ta$) (ICDD File 48–558) and $SrTiO_3$ (ICDD File 35–734) is formed, as it is evident from Figs. 1 and 2. The synthesizing conditions, and a summary of lattice parameters, cell volume, density, and tolerance factor of $Ca_{5-x}Sr_xA_2TiO_{12}$ ($0 \leqslant x \leqslant 4$) and $Sr_4A_2O_9 - SrTiO_3$ ceramics are given in Tables I and II, respectively, for $A=Nb$ and Ta.

It is evident from the tables that the substitution of Sr for Ca in the perovskite A site increases the lattice parameters and cell volume. We remark that for $x=2$, 3, and 4 the superstructure volumes were calculated into the cubic perovskite framework, for which the atomicity is $Z=1$, whereas for the orthorhombic group $Z=4$. Hence, to be in line with the cell volume of orthorhombic structures, the unit cell volumes of the pseudocubic structures were multiplied by 4. In

TABLE II. Synthesizing conditions, lattice parameters, cell volume, density, and tolerance factor of $Ca_{5-x}Sr_xTa_2TiO_{12}$ ($0 \leqslant x \leqslant 4$) and $Sr_4Ta_2O_9 - SrTiO_3$ ceramics.

| | Calcination temperature (°C) | Sintering temperature (°C) | Structure of the unit cell | Lattice parameters (Å) [Standard deviation SD=±0.0002 Å] | | | Cell volume (Å³) | Theoretical density (g/cm³) | % Density | Tolerance factor (t) |
x				a	b	c				
0	1350	1625	Orthorhombic	5.502 2	7.893 1	5.668 5	246.179 6	5.41	97.22	0.918 9
1	1300	1625	Orthorhombic	5.588 9	7.957 7	5.668 8	252.121 6	5.60	97.39	0.927 3
2	1300	1600	Pseudocubic	3.990 6	⋯	⋯	254.196 6	5.86	96.76	0.935 7
3	1250	1575	Pseudocubic	4.014 6	⋯	⋯	258.815 6	6.06	96.53	0.944 1
4	1250	1550	Pseudocubic	4.044 9	⋯	⋯	264.724 4	6.23	98.59	0.952 5
5	1275	1560	Mixture ($Sr_4Ta_2O_9-SrTiO_3$)	a	a	a	a	a	a	a

[a]Could not be calculated because of the mixed-phase nature.
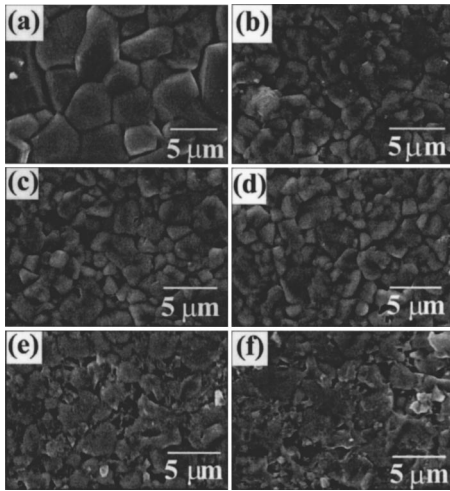
FIG. 3. SEM pictures of (a) $Ca_5Nb_2TiO_{12}$, (b) $Ca_3Sr_2Ta_2TiO_{12}$, (c) $CaSr_4Nb_2TiO_{12}$, (d) $CaSr_4Ta_2TiO_{12}$, (e) $Sr_4Nb_2O_9-SrTiO_3$, and (f) $Sr_4Ta_2O_9-SrTiO_3$ ceramics.

$Ca_{5-x}Sr_xNb_2TiO_{12}$ ceramics the theoretical density varies from 4.19 to 5.13 g/cm^3 as x changes from 0 to 4, and the experimental density reaches more than 97% of the theoretical value. $Ca_{5-x}Sr_xTa_2TiO_{12}$ has also an experimental density of about 97%, where the theoretical density varies from 5.41 to 6.23 g/cm^3 as x takes the value from 0 to 4. The increase in density with x is quite expected, as the molecular weight of Sr is higher than that of Ca. The tolerance factor t,[38] which is a measure of the symmetry of the perovskite structure, is calculated for the investigated ceramic systems using the relation

$$t = \frac{R_O + [R_{Ca}(4-x)/4] + (R_{Sr}x/4)}{\sqrt{2}[R_O + (0.25R_{Ca} + 0.50R_{Nb/Ta} + 0.25R_{Ti})]},$$

where R denotes the radius of corresponding cations occupying the appropriate perovskite sites. The increase in average A-site ionic radius is associated with enhancement in tolerance factor, and the symmetry approaches cubic when $t \rightarrow 1$ (theoretically). From Tables I and II it is clear that with the increase of strontium content the tolerance factor increases and approaches unity.

B. Microstructural analysis

SEM micrographs of polished and thermally etched surfaces of the sintered samples are shown in Fig. 3. Size and shape of the grains vary with the concentration of Sr^{2+} content, and presents a uniform distribution in all cases. In Fig. 3(a) the surface morphology of the $Ca_5Nb_2TiO_{12}$ ceramics sintered at 1550 °C is shown, which has an average grain size of 6–7 μm. Figures 3(b)–3(d) depict the microstructure of $Ca_3Sr_2Ta_2TiO_{12}$, $CaSr_4Nb_2TiO_{12}$, and $CaSr_4Ta_2TiO_{12}$ ceramics, respectively.

It is evident from the figures that their average grain size is about 1–2 μm, which is much less than that of $Ca_5Nb_2TiO_{12}$ ceramics [see Fig. 3(a)]. This implies that the substitution of Sr^{2+} with Ca^{2+} improves the sinterability and enhances densification (see Tables I and II). A pronounced difference in microstructure is not observed between the

samples shown in Fig. 3(a) and those in Figs. 3(b)–3(d). However, in Figs. 3(a)–3(d), no secondary phases can be observed in any specimen, and complete solid solution of the complex perovskite phase was confirmed for $x=0$ to 4. Figures 3(e) and 3(f) show nonuniform microstructure, with pores in the grain boundaries. The complete substitution of Sr^{2+} in place of Ca^{2+} ions in $Ca_5A_2TiO_{12}$ ($A=Nb,Ta$) results in the formation of a mixture phase, as is evident from the presence of two distinct types of grains [$Sr_4A_2O_9$ ($A=Nb,Ta$) and $SrTiO_3$] in Figs. 3(e) and 3(f). The similarity between microstructural evolution in niobium- and tantalum-based specimens are quite evident by comparing Figs. 3(c) and 3(d) with 3(e) and 3(f). In all the cases the SEM pictures are in good agreement with the structural analysis using XRD.

C. Microwave dielectric properties

The microwave dielectric properties of $Ca_{5-x}Sr_xNb_2TiO_{12}$ ceramics with different mole fractions of strontium content are given in Fig. 4. The quality factor varies from 26 000 GHz (at 4 GHz) to 6000 GHz (at 3 GHz) when x changes from 0 to 3. $Q_u \times f$ increases abruptly to 11 000 GHz for $x=4$. In $Ca_{5-x}Sr_xNb_2TiO_{12}$ ceramics, when $x=0$ and $x=4$ the perovskite A site is completely occupied by either Ca (for $x=0$) or Sr (for $x=4$) ions and has higher $Q_u \times f$ compared to other compositions from $x=1$ to 3, where partial occupancy of Ca and Sr ions takes place in the perovskite A site (double perovskite structure).

Moreover, it is evident from Fig. 4 that the quality factor is higher for $x=0$ than that of $x=4$. The replacement of the larger Sr ion with the comparatively smaller Ca ions in the perovskite A site leads to distortions in the unit cell, and hence structural phase transition occurs, which causes the reduction of the quality factor for $Sr(Ca_{1/4}A_{2/4}Ti_{1/4})O_3$ ($A=Nb,Ta$) ceramics compared with $Ca(Ca_{1/4}A_{2/4}Ti_{1/4})O_3$ ($A=Nb,Ta$). For all other compositions ($x=1$, 2, and 3), the structural transformations due to the substitution reaction reduces the quality factor. For $x=5$ the multiphase compound which is a mixture of $Sr_4Nb_2O_9$ and $SrTiO_3$ was formed, and it did not resonate. The dielectric constant and τ_f of $Ca_{5-x}Sr_xNb_2TiO_{12}$ increases with strontium content. It is quite expected as the dielectric polarisability of Sr is higher than that of Ca.[39] The microwave dielectric properties of $Ca_{5-x}Sr_xTa_2TiO_{12}$ ($0 \leq x \leq 4$) are shown in Fig. 5.

The quality factor gradually decreases from $x=0$ to $x=3$, and then increases for $x=4$. $Q_u \times f$ changes from 33 000 GHz (at 5 GHz) to 8500 GHz (at 4 GHz) and reaches 16 000 GHz (at 3.8 GHz) for $x=4$, i.e., $Sr(Ca_{1/4}Ta_{2/4}Ti_{1/4})O_3$. The behavior is similar to that exhibited by their niobium analogue. The ε_r varies from 38 to 46 as x changes from 0 to 4, and τ_f shifts to the more positive side and reaches 21 ppm/°C for $x=4$. The properties like cell volume, density, tolerance factor, ε_r, and τ_f show linear variations with x, whereas $Q_u \times f$ decreases from $x=0$ to $x=3$, and then increases for $x=4$. In this case also compositions with single occupancy of the perovskite A site either by Ca (for $x=0$) or Sr (for $x=4$) show higher Q_u compared to
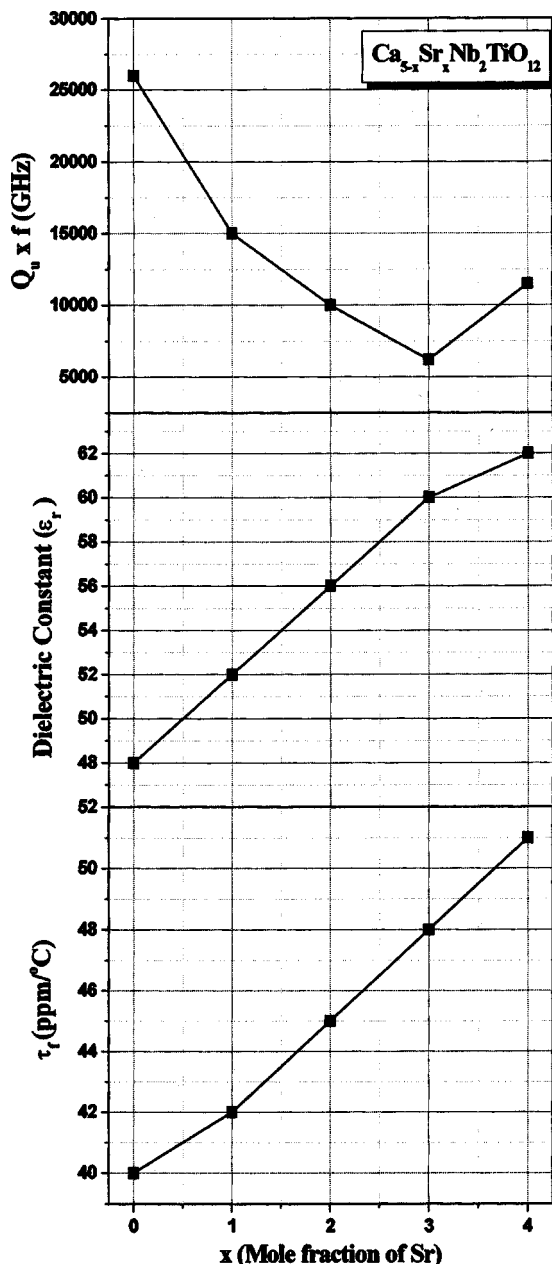
FIG. 4. Variation of microwave dielectric properties of $Ca_{5-x}Sr_xNb_2TiO_{12}$ $(0 \leqslant x \leqslant 4)$ ceramics with mole fraction of Sr content.

FIG. 5. Variation of microwave dielectric properties of $Ca_{5-x}Sr_xTa_2TiO_{12}$ $(0 \leqslant x \leqslant 4)$ ceramics with mole fraction of Sr content.

other compositions ($x=1$ to 3), where coexistence of the above-mentioned cations takes place in the A site.

D. Raman spectroscopic studies

Figures 6 and 7 present the Raman spectra for $Ca_{5-x}Sr_xNb_2TiO_{12}$ and $Ca_{5-x}Sr_xTa_2TiO_{12}$ $(0 \leqslant x \leqslant 5)$ microwave ceramics, with isovalent cation substitution on the A site. In both figures with $x=0$, the spectra can be interpreted as a combination of the typical Raman spectra of the end members $CaTiO_3$ and $Ca_4Nb_2O_9$ or $Ca_4Ta_2O_9$. Here, we have characteristic bands of A sites occupied by Ca ($117-123$ cm^{-1}) and a complex set of bands related to the B sites, which present an average $Ca_{1/4}Nb_{1/2}Ti_{1/4}$ and $Ca_{1/4}Ta_{1/2}Ti_{1/4}$ occupancy. The broad band observed at 640 cm^{-1} can be assigned to the B-O symmetric stretching
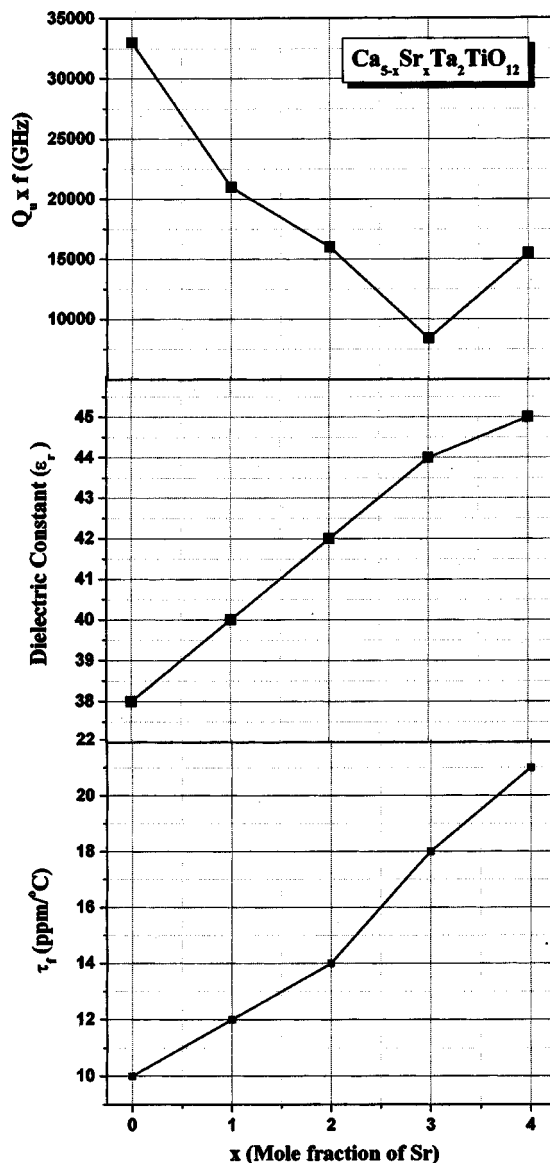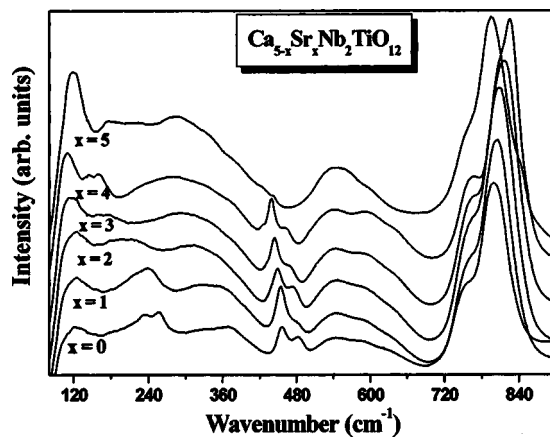

FIG. 6. Raman results of $Ca_{5-x}Sr_xNb_2TiO_{12}$ complex perovskites, with isovalent substitution of Sr for Ca.
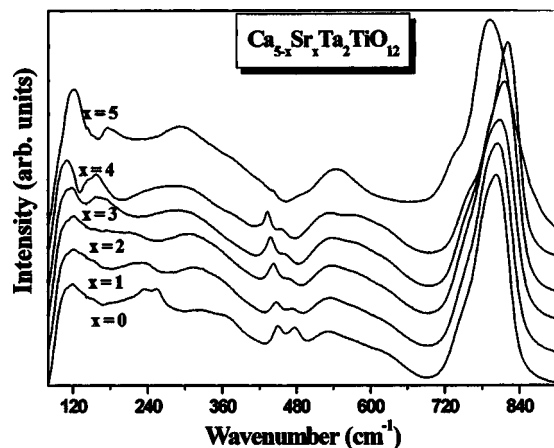
FIG. 7. Raman results of $Ca_{5-x}Sr_xTa_2TiO_{12}$ complex perovskites, with isovalent substitution of Sr for Ca.

vibration.[40–42] The bands at 450–455 and 475–485 cm^{-1} are assigned to the B-O_3 torsional (bending or internal vibration of oxygen cage) modes, although the frequencies verified in similar perovskites were higher.[40–42] This behavior can be understood as an effect caused by the more distorted coordination environment of B sites due to the presence of Ca, Nb/Ta, and Ti in the solid solutions. The bands in the region 235–370 cm^{-1} are related to the modes associated with rotations of oxygen cage and B-site ordering.[42] The bands at 530–600 and 750–800 cm^{-1} correspond to oxygen motion (A_{1g} mode), which can be represented as symmetric and asymmetric "breathing" of the BO_6 octahedra, respectively. Concerning ordering, it is clear that the bands in the regions 300–400 and 750–800 cm^{-1} are related to 1:1 ordering, similar to the results of Raman spectroscopic studies carried out by Levin *et al.*[43] and Zheng *et al.*[42] in $Ca(Ca_{1/3}Nb_{2/3})O_3$- and $CaTiO_3$-based ceramics, respectively. According to the group-theory analysis for 1:1 superstructures with $Fm3m$ and 1:2 ordered perovskites with $P\bar{3}m1$ space group, A_{1g} and F_{2g} modes become Raman active due to B-site ordering.[44,45] The substitution of Nb by Ta in Fig. 7 with $x=0$ produced a faint shift to lower frequencies (redshift), as expected. However, an exception has occurred at 798–803 cm^{-1}, corresponding to the A_{1g}(O) mode, which blueshifted for the ceramic with tantalum. This behavior can be explained by the increase of the force constant or the stiffness of the oxygen octahedra cage, as also verified by Siny *et al.* in $Ba(Mg_{1/3}Ta_{2/3})O_3$ ceramics.[44] Also, the increase in the intensity of the bands at 375 and 750 cm^{-1} for compounds with Nb are probably related to a higher short-range ordering. Similar results were observed by Zheng *et al.*[42] for the system $CaTiO_3$-$Sr(Mg_{1/3}Nb_{2/3})O_3$.

With Sr substitution, we note first that the spectra for $x=0$ to 4 show all the same number of features. This is compatible with the interpretation that although the structure evolves to pseudocubic for higher x values, it remains orthorhombic. The region below 300 cm^{-1} presented interesting changes with Sr substitution. The bands centered at 98 (Nb) and 93 cm^{-1} (Ta) shifted to lower frequencies with the introduction of Sr for x up to 4. Also, the peaks at 265 (Nb) and 255 cm^{-1} (Ta) decreased their intensity and became broader

at higher frequencies for increasing x. When $x=4$, bands appeared at 140–160 cm^{-1} in Nb-based ceramics and at 135–155 cm^{-1} in Ta-based compounds as a result of a highly distorted structure. These last bands disappeared for the materials with $x=5$, and a final shift to higher frequencies occurred for the band at around 95 cm^{-1}, which moved to 118 (Nb) and to 115 cm^{-1} (Ta), and the spectra looked different from that of all other compositions. It is in agreement with the XRD pattern that with $x=5$, $Sr_5(Nb/Ta)_2TiO_{12}$ does not form, but it is a mixture of $SrTiO_3$ and $Sr_4(Nb/Ta)_2O_9$. From Figs. 6 and 7, it is evident that the band at 117–123 cm^{-1} is shifted to higher frequencies with increase in x. This region of the spectra reflects the A-site environment, as well as probable rotations of the oxygen cage. These results are also in line with the structural characterization that the substitution of strontium by calcium occurs in the perovskite A site, which causes strong effects in the band at 117–123 cm^{-1}. These effects result from the more pronounced distortions in the oxygen octahedra due to the size difference between the isovalent cations Ca and Sr. Increasing the amount of strontium atoms ($1 \leqslant x \leqslant 4$), now in A sites, led to higher distortions, shifting the bands continuously to lower frequencies. This behavior is related to the increased global mass in the A site due to the substitution of heavier Sr^{2+} ions in the mixed complex ceramics. On the other hand, the A_{1g}(O) mode shifted to higher frequencies for increasing Sr content as a result of the volume change (rather than mass), which increased for ceramics with more Sr (see density values in Table I and II). Microwave properties showed interesting results for $x=4$ (Figs. 4 and 5), with a sudden increase in Q_u probably associated to the distortions in the octahedra verified by Raman spectroscopy.

The region 300–900 cm^{-1} presented similar behavior for both $Ca_{5-x}Sr_xNb_2TiO_{12}$ and $Ca_{5-x}Sr_xTa_2TiO_{12}$ materials. The most important variations were observed in the bands centered at 455–482 cm^{-1} in niobium-based materials (see Fig. 6) and 450–478 cm^{-1} in the tantalum analogue (see Fig. 7). The variations are assigned to BO_3 torsional modes, which shifted continuously to lower values for $x=0$ to 4, together with a decrease of the second band. But both these bands disappeared for $x=5$. This behavior can be explained if one considers that the larger and heavier Sr^{2+} interacts with anions less strongly, so reducing the distortion of the octahedra and also of the cell volume (increased densities with x). Similarly, the bands in the region 540–660 cm^{-1} presented the same behavior, and also increased their intensities with Sr introduction. On the contrary, the breathing modes centered at around 800 cm^{-1} shifted to higher frequencies with Sr substitution by more than 20 cm^{-1} when $x=4$. But with $x=5$, the same mode returns to low frequency and appears at 795 cm^{-1}. The mixture phase formation of $Ca_{5-x}Sr_xNb_2TiO_{12}$ and $Ca_{5-x}Sr_xTa_2TiO_{12}$ with $x=5$ is verified in the Raman spectroscopy by the unusual behavior of shifting and disappearance of certain modes. Thus substituting Sr^{2+} for Ca^{2+} caused tilting and distortions in the oxygen cages. In the present work, the presence of only one calcium in the B sites and complete substitution of Ca with Sr in the perovskite A site when $x=4$ lead to maximum distortion, which activated

forbidden Raman modes at 140–160 cm^{-1} in Ca$_{5-x}$Sr$_x$Nb$_2$TiO$_{12}$ ceramics and at 135–155 cm^{-1} for Ca$_{5-x}$Sr$_x$Ta$_2$TiO$_{12}$ (see Figs. 6 and 7).

The A_{1g}(O) mode represents a qualitative indication of the degree of B-site ordering and, obviously, differences in charge or ionic sizes will influence the distribution of ions on any given site. Ca and Sr atoms present significant differences in their ionic sizes[36] and the larger the difference, the greater the influence on the vibrational modes, particularly those related to ordering. Zheng *et al.*[46] considered the possibility that the width and the frequency of the A_{1g}(O)-mode band may be affected by the size distribution of the A-site cations. Their conclusions are that the A-site ionic distribution influences the degree of short-range order on the B site or, also, the size differences in the A site could constrict in some manner the octahedra breathing mode to occur in a given range of frequencies. In our case, it is believed that the A_{1g}(O) mode is a function of the volume cage, which presents the maximum variation for $x=4$ (complete replacement of Ca with Sr in the A site). Finally, correlating this result to the microwave properties, the decrease in Q_u with Sr introduction (see Figs. 4 and 5) could be an expected result, because its presence alters A-site distribution and probably increases the degree of short-range order. This increase is detrimental to Q_u because it induces anharmonicity and increases phonon damping. Zheng *et al.*[46] and Webb *et al.*[47] reported that the values of Q_u must increase only when the order changes from short to long range. In this respect, it is interesting to observe the increase in Q_u for $x=4$, with complete introduction of Sr in the perovskite A site which probably leads to a long-range order at this composition. The mode at 240 cm^{-1} for $x=0$ for both niobates and tantalates shifts to the low-frequency side as x increases. The band almost disappears for $x=1$, 2, and 3, but reappears for $x=4$. This is in agreement with the assumption that with $x=0$ and $x=4$ the perovskite A site is occupied by single ions. When $x=0$, Ca^{2+} ions and with $x=4$, Sr^{2+} ions occupy the perovskite A site, and both compositions have high quality factor. But the difference in ionic radius between the two produces lattice distortions and resultant structural changes, which was verified by XRD as well as Raman spectroscopic studies.

E. FTIR analysis

FTIR results agree well with Raman spectroscopic data, either concerning the conclusions on the structural evolution or on the dependence of vibrational features with cation substitutions. Figures 8 and 9 present the results of FTIR analyses for Ca and Sr mixed-microwave ceramics. As can be seen from Fig. 8, with $x=0$ the Nb- and Ta-based compounds showed important differences, including a more defined set of bands at 220, 265, 318, 370, 396, 470, 540, 570, and 670 cm^{-1}. The frequency region below 150 cm^{-1} can be attributed to the A-BO_3 external mode, while the O-B-O bending modes appear between 170 and 500 cm^{-1}.[48] The highest wave number range, 500–700 cm^{-1}, is due to the oxygen octahedra-elongation mode; that is, BO_6 stretching. Tantalum substitution leads to shifting of lower frequencies as expected, as well as increasing the intensities of the bands at
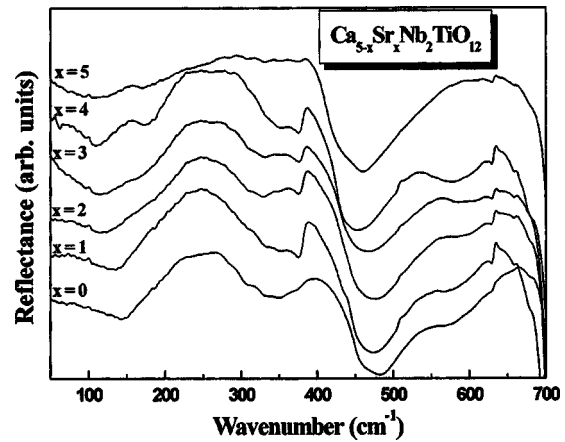

FIG. 8. FTIR results of Ca$_{5-x}$Sr$_x$Nb$_2$TiO$_{12}$ complex perovskites, with isovalent substitution of Sr for Ca.

370, 470, and 540 cm^{-1}. This behavior can be associated to the stiffness of the oxygen octahedra in Ca$_5$Ta$_2$TiO$_{12}$ ceramics. Bands below 100 cm^{-1} and above 600 cm^{-1} are difficult to assign due to instabilities in the measurements, with consequent poor quality.

The spectra of both niobates and tantalates show similar behavior. Strontium substitution leads to a better definition of the bands at around 150 cm^{-1} and in the range 220–320 cm^{-1}, with a maximum at $x=4$. Also, lattice distortions caused by substitution of Ca by Sr increased the band at 350–360 cm^{-1}. Shifts occurred especially in the dip, centered at 490 cm^{-1} for Nb-based ceramics (see Fig. 8) and at 480 cm^{-1} for Ta ceramics (see Fig. 9). Also, it is interesting to note the increase of the band at 550 cm^{-1}, which is related to the oxygen octahedral-elongation modes. Stronger bands at 150 and 220–320 cm^{-1} are as a result of the perturbations in the O-metal-O bending modes (inner mode vibrations) on the B sites, as well as in the band at around 350 cm^{-1}. The maximum distortions at $x=4$ coincide with the sudden increase observed in Q_u, and verified with the particular features formed in Raman spectra. This frequency range can be considered as specific for ordered structures, and their strength can be used as a relative measure of this ordering.[48] The frequency shifts observed around 480 and 550 cm^{-1} in the FTIR spectra can be related to the BO_3 torsional (ν_2) and
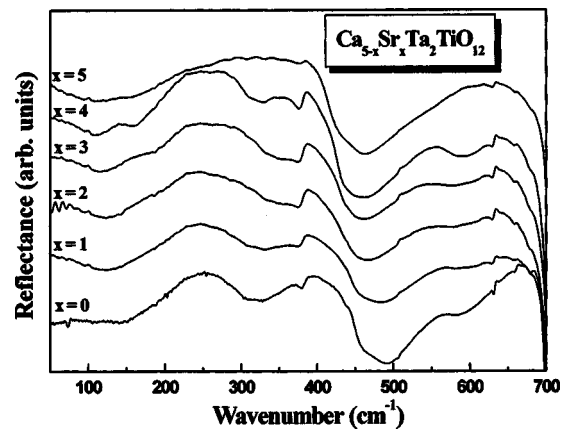

FIG. 9. FTIR results of Ca$_{5-x}$Sr$_x$Ta$_2$TiO$_{12}$ complex perovskites, with isovalent substitution of Sr for Ca.

the BO stretching (ν_1) modes. It confirms the hypothesis that the Sr substitution occurs on the *A* site of the complex perovskite material.

IV. CONCLUSIONS

$Ca_{5-x}Sr_xA_2TiO_{12}$ (A=Nb,Ta) complex perovskite-type ceramics have been prepared as single-phase materials up to x=4. The structure, microwave dielectric properties, and Raman and FTIR studies have been reported. The ceramics undergo a structural evolution with increasing x. For x=0 and 1, they exist in a clear perovskite orthorhombic symmetry. For x=2 to 4, it evolves to a pseudocubic structure, with a negligible difference between lattice parameters, but the orthorhombic true symmetry of which is revealed by spectroscopic data. The structural evolution is followed by changes in the unloaded quality factor of the dielectrics. In both niobates and tantalates, Q_u showed a gradual decrease for x=0 to 3 (26 000–6000 GHz for Nb compounds and 33 000–8500 GHz for Ta-based ceramics) and then increased for x=4 (11 500 GHz for Nb- and 16 000 GHz for Ta-based materials). Raman results showed that materials with Ta ions differ from those with Nb ions only by shifts to lower frequencies (redshift). An exception occurred at the $A_{1g}(O)$ mode, which blueshifted for the ceramics with Ta atom as a result of the higher stiffness of the oxygen octahedral cage. Isovalent Sr substitution on Ca-based samples led to rotations of the oxygen cage that redshifted the bands related to the *A* sites. Modes related to ordering varied their intensities and frequencies as a result of the increased short-range order. Maximum distortions occurred at x=4 in the octahedral cages, which lead to the unexpected increase in Q_u, probably due to a long-range order. FTIR results agree well with Raman data; introduction of strontium in calcium-based ceramics produced perturbations on the polar vibrational modes, especially on the bending modes, which increased their intensities.

ACKNOWLEDGMENTS

[1] D. Kajfez and P. Guillon, *Dielectric Resonators* (Artech House, Massachusetts, 1986).
[2] W. Wersing, *Electronic Ceramics*, edited by B. C. H. Steele (Elsevier, Amsterdam, 1991), p. 67.
[3] A. I. Kingon, J. P. Maria, and S. K. Streiffer, Nature (London) **406**, 1032 (2000).
[4] Y. Kawashima, M. Nishida, J. Ueda, and H. Ouchi, J. Am. Ceram. Soc. **66**, 421 (1983).
[5] S. Kawashima, Am. Ceram. Soc. Bull. **75**, 120 (1993).
[6] S. B. Desu and H. M. O'Bryan, J. Am. Ceram. Soc. **68**, 546 (1985).
[7] J.-W. Choi, J.-Y. Ha, C.-Y. Kang, S.-J. Yoon, H.-J. Kim, and K. H. Yoon, Jpn. J. Appl. Phys., Part 1 **39**, 5923 (2000).
[8] N. Santha *et al.*, J. Am. Ceram. Soc. **87**, 1233 (2004).
[9] K. P. Surendran, Manoj R. Varma, M. T. Sebastian, and P. Mohanan, J. Mater. Res. **17**, 2561 (2002).
[10] S. K. Kucheiko, D.-H. Yeo, J.-W. Choi, S.-J. Yoon, and H.-J. Kim, J. Am. Ceram. Soc. **85**, 1327 (2002).
[11] P. Liu, E. S. Kim, S. G. Kang, and H. S. Jang, Mater. Chem. Phys. **79**, 270 (2003).
[12] G. Huang, D. Zhou, J. Xu, X. Chen, D. Zhang, W. Lu, and B. Li, Mater. Sci. Eng., B **99**, 416 (2003).
[13] H. Jantunen, R. Rautioaho, A. Uusimaki, and S. Leppavuri, J. Eur. Ceram. Soc. **20**, 2331 (2000).
[14] A. Y. Borisevich and P. K. Davies, J. Am. Ceram. Soc. **85**, 573 (2002).
[15] M.-H. Kim, S. Nahm, C.-H. Choi, H.-J. Lee, and H.-M. Park, Jpn. J. Appl. Phys., Part 1 **41**, 717 (2002).
[16] M. T. Sebastian, N. Santha, P. V. Bijumon, Anna Axelsson, and Neil McN Alford, J. Eur. Ceram. Soc. **24**, 2583 (2004).
[17] K. P. Surendran, Manoj R. Varma, M. T. Sebastian, and P. Mohanan, J. Am. Ceram. Soc. **86**, 1695 (2003).
[18] I. Levin, T. A. Vanderah, and R. Coutts, J. Mater. Res. **17**, 1729 (2002).
[19] http://www.lsbu.ac.uk/dielectric-materials
[20] R. J. Cava, J. J. Krajewski, and R. S. Roth, Mater. Res. Bull. **34**, 355 (1999).
[21] L. A. Bendersky, J. J. Krajewski, and R. J. Cava, J. Eur. Ceram. Soc. **21**, 2653 (2001).
[22] P. V. Bijumon, P. Mohanan, and M. T. Sebastian, Jpn. J. Appl. Phys., Part 1 **41**, 3834 (2002).
[23] P. V. Bijumon, P. Mohanan, and M. T. Sebastian, Mater. Lett. **57**, 1380 (2003).
[24] L. A. Bendersky, I. Levin, R. S. Roth, and A. J. Shapiro, J. Solid State Chem. **160**, 257 (2001).
[25] P. V. Bijumon and M. T. Sebastian, J. Mater. Res. **19**, 2922 (2004).
[26] P. V. Bijumon and M. T. Sebastian (unpublished results).
[27] P. V. Bijumon, Sreedevi K. Menon, P. Mohanan, and M. T. Sebastian, Microwave Opt. Technol. Lett. **35**, 327 (2002).
[28] S. Mridula, Sreedevi K. Menon, P. Mohanan, P. V. Bijumon, and M. T. Sebastian, Microwave Opt. Technol. Lett. **40**, 316 (2004).
[29] T. Simada, J. Eur. Ceram. Soc. **21**, 2617 (2001).
[30] H. Bagshaw, D. Iddles, R. Quimby, and I. M. Reaney, J. Eur. Ceram. Soc. **23**, 2435 (2003).
[31] P. L. Wise, I. M. Reaney, W. E. Lee, T. J. Price, D. M. Iddles, and D. S. Cannell, J. Eur. Ceram. Soc. **21**, 1723 (2001).
[32] J. Krupka, K. Derzakowski, B. Riddle, and J. B. Jarvis, Meas. Sci. Technol. **9**, 1751 (1998).
[33] B. W. Hakki and P. D. Coleman, IEEE Trans. Microwave Theory Tech. **MTT-18**, 402 (1960).
[34] W. E. Courtney, IEEE Trans. Microwave Theory Tech. **MTT-18**, 476 (1970).
[35] A. M. Glazer, Acta Crystallogr., Sect. B: Struct. Crystallogr. Cryst. Chem. **28**, 3384 (1972).
[36] R. D. Shannon, Acta Crystallogr., Sect. A: Cryst. Phys., Diffr., Theor. Gen. Crystallogr. **32**, 751 (1976).
[37] M. A. Akbas and P. K. Davies, J. Am. Ceram. Soc. **81**, 2205 (1998).
[38] R. S. Roth, J. Res. Natl. Bur. Stand. **58**, 75 (1957).
[39] R. D. Shannon, J. Appl. Phys. **73**, 348 (1993).
[40] T. Hirata, K. Ishioka, and M. Kitasima, J. Solid State Chem. **124**, 353 (1996).
[41] U. Balachnadran and N. G. Eror, Solid State Commun. **44**, 815 (1982).
[42] H. Zheng, G. D. C. Csete de Gyorgyfalva, R. Quimby, H. Bagshaw, R. Ubic, I. M. Reaney, and J. Yarwood, J. Eur. Ceram. Soc. **23**, 2653 (2003).
[43] I. Levin, J. Y. Chan, R. G. Geyer, J. E. Maslar, and T. A. Vanderah, J. Solid State Chem. **156**, 122 (2001).
[44] I. G. Siny, R. Tao, R. S. Katiyar, R. Guo, and A. S. Bhalla, J. Phys. Chem. Solids **59**, 181 (1998).
[45] H. Zheng, I. M. Reaney, G. D. C. Csete de Gyorgyfalva, R. Ubic, J. Yarwood, M. P. Seabra, and V. M. Ferreira, J. Mater. Res. **19**, 488 (2004).
[46] H. Zheng, H. Bagshaw, G. D. C. Csete de Gyorgyfalva, I. M. Reaney, R. Ubic, and J. Yarwood, J. Appl. Phys. **94**, 2948 (2003).
[47] S. J. Webb, J. Breeze, R. I. Scott, D. S. Cannell, D. M. Iddles, and N. McN Alford, J. Am. Ceram. Soc. **85**, 1753 (2002).
[48] A. Dias and R. L. Moreira, J. Appl. Phys. **94**, 3414 (2003).